ACS APPLIED NANO MATERIALS

www.acsanm.org Article

Protective Coatings Based on Cellulose Nanofibrils, Cellulose Nanocrystals, and Lignin Nanoparticles for the Conservation of Cellulosic Artifacts

Camilla H. M. Camargos, Giovanna Poggi, David Chelazzi, Piero Baglioni, and Camila A. Rezende*

Cite This: *ACS Appl. Nano Mater.* 2022, 5, 13245−13259 Read Online

ACCESS | Metrics & More | Article Recommendations | Supporting Information

ABSTRACT: Green nanocomposites combining cellulose nanofibrils (CNFs), cellulose nanocrystals (CNCs), and lignin nanoparticles (LNPs) were designed and applied for the first time as ternary protective coatings on cellulosic materials, i.e., substrates mainly composed of cellulose. All the nanostructures were obtained from elephant grass biomass. CNFs and CNCs are less than 10 nm thick and present a filament-like morphology, while LNPs are spheres with an average diameter of less than 100 nm. The use of water-based nanoparticle dispersions is a facile and greener alternative to synthetic varnishes usually based on toxic organic solvents. Moreover, the coatings from renewable sources were chemically stable; showed high compatibility with wood, paper, and fabric; and preserved the roughness and surface morphology of the substrates after application. Moist-heat accelerated aging and UV-shielding assays revealed that the nanocellulose/nanolignin coatings were able to protect the coated cellulosic substrates against degradation. The wettability of nanocomposite-coated substrates could be tailored and reduced to produce hydrophobic surfaces by applying additional layers of water-based carnauba wax nanoparticles, which are also sustainable. Additionally, two-dimensional infrared spectroscopy mapping confirmed the reversibility of the coating application, as the nanocomposite layers could be easily removed from the cellulosic substrates by water-loaded cleaning hydrogels. Therefore, the functional protective coating introduced here represents an environmentally friendly and nontoxic approach for the conservation of cellulosic artifacts in general, including cultural heritage objects based on paper, wood, and fabric.

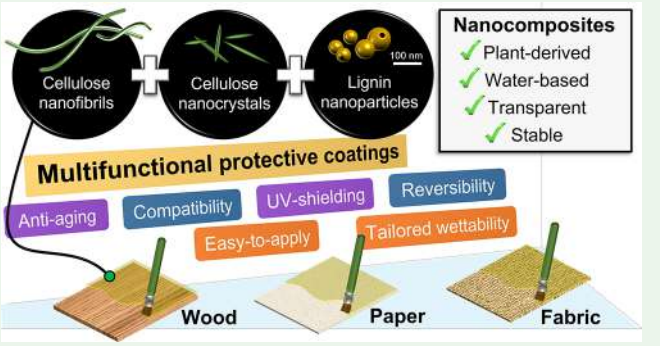

KEYWORDS: *wood, paper, fabric, cellulose nanofibrils, cellulose nanocrystals, lignin nanoparticles, elephant grass, protective coating*

INTRODUCTION

Lignocellulosic biomasses such as grasses, softwoods, and hardwoods can be converted into nanocelluloses, including cellulose nanocrystals (CNCs) and cellulose nanofibrils (CNFs), as well as into nanolignins, which are also referred to as lignin nanoparticles (LNPs). CNCs are rigid, highly crystalline, needle-like nanoparticles, while CNFs are flexible filaments with a semicrystalline nature; i.e., they contain interspersed crystalline and amorphous fractions. Both CNCs and CNFs present an average width of less than 10 nm, but the former are generally shorter (*ca.* 150−300 nm in length) than the latter (600−1300 nm in length).[1] LNPs, on the other hand, are usually obtained as soft core−shell nanospheres with *ca.* 100 nm.[2] Currently, these nanostructures are applied in numerous multifunctional materials, comprising nanocomposites,[3−5] films,[6] foams,[7] and membranes.[8] Additionally, nanocelluloses and nanolignins—alone or combined with other organic or inorganic species—have often been separately applied as consolidants or coatings on polymeric packaging[9] and wood,[10−14] paper,[15−22] and fabric[23−26] substrates.

This versatility of applications arises from the intrinsic properties of the nanostructures, such as high tensile strength, stiffness, biocompatibility, gas barrier,[6] and optical transparency of nanocelluloses,[1] and antimicrobial, antioxidant, and UV-blocking properties of nanolignins.[2] Moreover, these renewable and high-value-added nanoparticles can be obtained from inexpensive and largely available crop residues or surpluses.[27] Nanocelluloses and nanolignins also present a natural compatibility[28] with each other and with cellulose-based substrates and to some extent an intrinsic biodegradability[5,29] unlike synthetic, nonrenewable, and petroleum-derived polymers. Additionally, such nanoparticles are

Received: July 8, 2022
Accepted: August 16, 2022
Published: August 29, 2022

colloidally stable and dispersible in water,[1,2] allowing for the preparation of less-toxic final products. Thus, they are promising problem-solving options to address a multitude of challenges, including those in the field of cellulose-based cultural heritage preservation.

The remedial conservation and restoration of cultural, artistic, and historical artifacts consist of directly treating the object's materiality,[30] i.e., its material structure. Protective protocols are developed with the purpose of extending the lifespan of the cultural object. Furthermore, these treatments aim to safeguard the original integrity[31] of the objects—from a physicochemical, aesthetic, historical, and informational standpoint. Therefore, preventing and slowing down degradation processes are results of paramount importance in such treatments, also when cellulose and lignin nanostructures are employed.

The use of lignin for conservation purposes can be received as quite controversial, since the presence of residual lignin has historically been pointed out as an intrinsic hindrance to the permanence of cellulosic materials, such as modern paper.[32] However, LNPs have already been introduced as consolidants for wooden archeological objects[11] or as protective shields for the wood surface,[14] and residual lignin has been shown to have no negative effect on the degradation of paper at neutral pH.[33] In fact, this complex macromolecule can mitigate the autoxidation of lignin-containing cellulose pulps, preventing strength losses[34] and inhibiting thermal degradation.[35] Lignin can cause thermal yellowing under an oxygen-rich atmosphere[34] or, conversely, hinder the water vapor enhanced degradation of pulp polysaccharides under hot humid conditions, minimizing chromophore formation.[35] Furthermore, nanolignin differs from residual, bulk lignin in multiple aspects: the former has a light brown/yellow coloration, is dispersible and colloidally stable in neutral aqueous media, and possesses higher UV-shielding and antioxidant efficiency than the latter, which presents a dark brown/black color and is poorly soluble.[2]

Here, we investigated the simultaneous combination of CNFs, CNCs, and LNPs to design advanced nanocomposite coatings useful for protecting diverse cellulose-based substrates, including those particularly associated with cultural heritage. As we demonstrated in a work,[36] we intended to merge the advantages of CNFs, CNCs, and LNPs while overcoming some inherent disadvantages. CNFs have interesting transparency, flexibility, and tensile strength, but self-standing CNF films often deform or shrink upon drying.[1] Conversely, transparent CNCs exhibit high crystallinity and chemical stability, but self-standing CNC films are usually too brittle[16] and shiny.[21] Due to the morphological, mechanical, and structural differences between the longer, flexible CNFs and the shorter, stiffer CNCs, when blended together, the transparent CNF/CNC films formed are flexible, flatter, more uniform, and less shiny than CNC-only films. The incorporation of LNPs, in turn, imparts a yellowish tint to the transparent films but contributes to provide antioxidant and UV protection capacity,[2] improving the colorimetric, thermal, and chemical stability of the nanocomposites.[36] All this in a waterborne formulation, avoiding the use of toxic solvents, such as turpentine and aromatics, usually required for the application of natural and synthetic resins as coatings.[37]

In this work, multifunctional protective coatings based on CNFs, CNCs, and LNPs were assessed and applied for the first time on wood, paper, and fabric mockups. We extensively evaluated the stability of the coatings and their protection against moist-heat aging and UV radiation. Additionally, their influence on mockup surface morphology and roughness, water vapor barrier properties, and tailored wettability were investigated. A more hydrophobic surface was obtained by applying additional layers of water-based carnauba wax nanoparticles (CWNPs), prepared by an adapted melting-sonication protocol.[38] We also addressed the reversibility or removability of the application by means of an assay of coating removal with a water-loaded hydrogel. The novel approach was proven to be promising as a sustainable, waterborne, and compatible strategy to protectively coat multiple cellulosic artifacts.

EXPERIMENTAL SECTION

Preparation of Nanocelluloses in Water. Cellulose fibers extracted from the leaves of elephant grass (*Pennisetum purpureum*) were converted into CNCs by the canonical acid hydrolysis method using 60 wt % H_2SO_4 at 45 ± 5 °C for 40 min, followed by purification steps by centrifugation. Conversely, CNFs were obtained from both the plant leaves and stems by oxidation with NaClO (4.5 g/g of cellulose) and TEMPO ((2,2,6,6-tetramethylpiperidin-1-yl)oxyl radical, 0.016 g/g of cellulose) and NaBr (0.1 g/g of cellulose) as catalysts at room temperature and under constant stirring for 130 min.[1] The oxidized pulp slurry was sequentially post-treated with 1 mol/L NaOH and 0.1 mol/L HCl, separately, according to a previously published protocol,[36] to remove unstable sodium anhydroglucuronate units and to convert sodium carboxylate into free carboxyl groups. Then, the material was probe-sonicated to promote its nanofibrillation into CNFs. Nanostructure morphology was analyzed by transmission electron microscopy (TEM) in a LIBRA 120 microscope (Carl Zeiss, Oberkochen, Germany). Details about these production methodologies and nanocellulose characterization can be found elsewhere.[1]

Preparation of Nanolignin in Water. Bulk lignin powder extracted from elephant grass leaves was solubilized in acetone solution (90 vol %) and converted into self-assembled LNPs by adding excess water as an antisolvent at room temperature. Nanostructure morphology was assessed by scanning electron microscopy (SEM) in a Quanta 250 FEG microscope (FEI, Hillsboro, USA). Details about this production methodology and nanolignin characterization can be found elsewhere.[2]

Preparation of Carnauba Wax Nanoparticles in Water. An adapted melting-dispersion procedure[38] was developed to prepare self-assembled CWNPs. Wax pellets were suspended in deionized water (1 wt %), and the system was heated up to 95 °C in a silicone oil bath. After the wax was completely melted on the surface of water, the system was probe-sonicated with a 220 W output (40% oscillation amplitude) and 20 kHz for 10 min (QR550, Eco-Sonics, Indaiatuba, Brazil). The white, opaque aqueous dispersion of CWNPs was vacuum filtered and diluted to 0.1 wt % prior to utilization. Nanoparticles were characterized by AFM (Shimadzu SPM 9600 microscope, Kyoto, Japan) and zeta potential measurements (Malvern Zetasizer Nano ZS-Zen 3600, Malvern, UK).

Preparation and Application of Coating Formulations. Nanocomposite coatings were prepared according to Table 1. As described in our previous work,[36] the CNF-to-CNC weight ratio was *ca.* 2:1 in all formulations. The total nanocellulose concentration in a dry basis varied from 100 to 90 wt %, while the LNP concentration

Table 1. Formulation of Nanocomposite Coatings in a Dry Weight Basis

film	CNFs (wt %)	CNCs (wt %)	LNPs (wt %)
NFC	66	34	0
NFCL1	65	34	1
NFCL10	60	30	10

https://doi.org/10.1021/acsanm.2c02968
ACS Appl. Nano Mater. 2022, 5, 13245−13259

ranged from 0 to 10 wt %. The CNF/CNC/LNP weight ratios were ∼2:1:0 in NFC, ∼2:1:0.03 in NFCL1, and 2:1:0.3 in NFCL10. Aqueous dispersions (pH 6−7) were combined to form mixtures with a fixed final concentration of 10 mg/mL. Afterward, the systems were homogenized using probe sonication with a 220 W output for 2 min.

Exclusively for the coating formulations destined to pliable textile substrates, some plasticizers were separately incorporated to prevent the surface layers from cracking or failing. Glycerol (GLY, MW: 92 g mol^{-1}), poly(ethylene glycol) (PEG, MW: 750 g mol^{-1}) or poly(propylene glycol) (PPG, MW: 4000 g mol^{-1}) were added to the aqueous dispersions of the NFCL1 formulation before homogenization at a concentration of 1 or 10 wt %, considering the final dry weight of the coating.

Fixed volumes of the mixtures, containing plasticizers or not, were brush-applied to form coating films with a 1 mg/cm^2 mass-to-area ratio on the surface of balsa wood (*Ochroma pyramidale*), white cotton paper (Canson Mi-Teintes, color code 335, 160 g/m^2 grammage, 60 wt % cotton rag content according to the supplier), and unbleached cotton fabric mockups (plain casement weave). The substrate average thicknesses were 1569 ± 19 μm for wood, 253 ± 7 μm for paper, and 395 ± 7 μm for cotton fabric. As confirmed by visual and haptic analyses, drying a 4 cm^2 coating area took up to 2 h at room temperature and approximately 50% relative humidity (RH). For comparison, 10 mg/mL Paraloid B72 (previously, Acryloid B72) in ethanol or toluene was similarly applied on wood, paper, and fabric. This copolymer of ethyl methacrylate and methyl acrylate is traditionally used as a transparent and stable varnish, adhesive, and finishing material suitable for metals, stone, glass, ceramics, wood,[39] paper,[40] paintings and textile conservation.[41] Although in most cases Paraloid B72 is not conventionally used as a permanent coating for pliable artifacts such as flexible papers, synthetic acrylic copolymers can be occasionally applied to consolidate and protect this type of substrate.[42]

Additionally, when specified, four layers of 1 mg/mL CWNPs were brush-applied onto the nanocomposite-coated substrates to improve their hydrophobicity.

Moist-Heat Accelerated Aging. Uncoated and coated cellulosic mockups were aged at moist-heat conditions (80 °C and ∼75% RH)[15,43] inside sealed vessels in an oven. The RH equilibrium was achieved using 58 wt % glycerol aqueous solutions[44] and confirmed at room temperature with a thermohygrometer.

UV-Irradiation Assay. Pure polypropylene (PP) samples with or without an overlay consisting of self-standing films made of Paraloid B72 or CNF/CNC/LNP nanocomposites were placed at a 12 cm distance from a UVA/UVB light source and irradiated for 168 h.[45] A detailed assay scheme is depicted in Figure S1. As a polyolefin, PP was used in this photo-oxidation experiment because the incorporation of oxygen atoms (carbonyl groups) into its structure can be easily tracked by spectroscopy techniques. Unaged and UV-aged PP samples were analyzed using ATR-FTIR (Agilent Cary 630 FTIR spectrometer, Santa Clara, USA).

Thickness Measurements. The average thickness of uncoated and coated substrates was estimated using a digimatic micrometer (Mitutoyo Corporation, Kanagawa, Japan) with a reading error of 1 μm. Measurements were performed in at least 10 random regions of each mockup in triplicate.

Water Vapor Permeability (WVP) Assay. Water vapor transmission rate (WVTR) and WVP of Paraloid B72, nanocomposite films, as well as uncoated and coated wood, paper, and fabric were measured using the "cup method" with adaptations.[46] The detailed procedure is presented in the Supporting Information with a detailed assay scheme in Figure S2.

Diffuse Reflectance Spectroscopy (DRS). The DRS spectra of self-standing film samples were collected in transmittance mode with a spectral resolution of 0.5 nm from 200 to 800 nm using a Shimadzu UV-2450 DRS spectrophotometer.

Colorimetric Measurements. Colorimetric coordinates of uncoated and coated substrates in the CIEL*a*b* color space were assessed using a portable X-RITE SP60 VIS spectrophotometer (Grand Rapids, USA) with an integration sphere, a D65 standard illuminant, and a 10° standard observer. The average parameters measured for at least six replicates of each pristine, uncoated mockup were as follows: wood (L^* = 79.7 ± 1.1; a^* = 4.8 ± 0.6; b^* = 14.6 ± 0.6), paper (L^* = 95.1 ± 0.1; a^* = − 0.6 ± 0.0; b^* = 4.6 ± 0.5), and fabric (L^* = 85.3 ± 0.3; a^* = 1.5 ± 0.1; b^* = 13.9 ± 0.7).

The color difference (ΔE)[47] between coated and uncoated substrates, as well as aged and unaged samples, was calculated using eq 1 below:

$$\Delta E_{Lab} = \sqrt{(\Delta L^*)^2 + (\Delta a^*)^2 + (\Delta b^*)^2} \quad (1)$$

where ΔL^*, Δa^*, and Δb^* are the variation in, respectively, the L^* coordinate (+lightness/−darkness), a^* contribution (+red/−green), and b^* contribution (+yellow/−blue). Measurements were performed at least in quadruplicate. An interpretation of the criteria of tolerance[47] accepted here follow the recommendations in eq 2, 3, 4, and 5 below:

$$0 < \Delta E \leq 2, \text{ color difference is not perceived or only slightly perceived} \quad (2)$$

$$2 < \Delta E \leq 3.5, \text{ color difference is moderately perceived} \quad (3)$$

$$5 < \Delta E \leq 5, \text{ an evident difference between colors is perceived} \quad (4)$$

$$5 < \Delta E, \text{ two different colors are perceived by an observer} \quad (5)$$

Surface Morphology Analyses. The surface morphology of uncoated and coated substrates was observed by SEM in an FEI SEM Inspect F50 operating at a 5 kV accelerating voltage with a secondary electron detector. Prior to the analysis, the samples were attached to SEM stubs using a conductive carbon tape and sputter coated with carbon in a Baltec SCD 050 Sputter Coater (Balzers, Liechtenstein) with a 2.5 A current. Additionally, the surface topology and roughness of uncoated and coated substrates were assessed by AFM using a Shimadzu SPM 9600 microscope. Topography (height) images were acquired in noncontact mode using an NCHR PointProbe Silicon SPM-Sensor (NanoWorld, Neuchâtel, Switzerland) with a tip curvature radius smaller than 8 nm, a cantilever with a force constant of 42 N m^{-1}, and a resonance frequency of 320 kHz. The average area roughness parameters (root-mean-square height, Sq, and arithmetical mean height, Sa) were calculated using the software Gwyddion (version 2.56) in two different areas per sample (10 × 10 and 5 × 5 μm^2).

Water Contact Angle (WCA) Measurements. The wettability of uncoated and coated substrates was determined using the sessile drop method with deionized water. The substrates were attached to glass microscope slides with a double-sided tape, and the water contact angles were measured using a Krüss EasyDrop goniometer (Hamburg, Germany). The analysis took 60 s, with one measurement every 10 s, and was performed five times at random locations on the substrates.

Removal Test. A chemical hydrogel consisting of semi-interpenetrated polymer networks of poly(hydroxyethyl methacrylate)/poly(vinylpyrrolidone), pHEMA/PVP,[48] was loaded with deionized water and used to adhere onto the coated surfaces to remove nanocomposite coatings in a 2 h cleaning process.

Two-Dimensional Infrared (2D Micro-FTIR) Spectroscopy Mapping. 2D micro-FTIR imaging of uncoated, coated, and cleaned mockups was carried out using an Agilent Cary 620−670 FTIR microscope equipped with a 128 × 128 focal plane array detector, in reflectance mode, with a pixel size of 5.5 × 5.5 μm^2, a spectral resolution of 4 cm^{-1}, and 128 scans per run. By screening the surface and collecting the spectra of uncoated and coated samples, variations in the integrated range from 1250 to 1155 cm^{-1} were detected and then used to obtain the surface mappings.

RESULTS AND DISCUSSION

Nanocellulose/Nanolignin-Based Nanocomposite Coatings. Taking advantage of the advanced mechanical

https://doi.org/10.1021/acsanm.2c02968
ACS Appl. Nano Mater. 2022, 5, 13245−13259

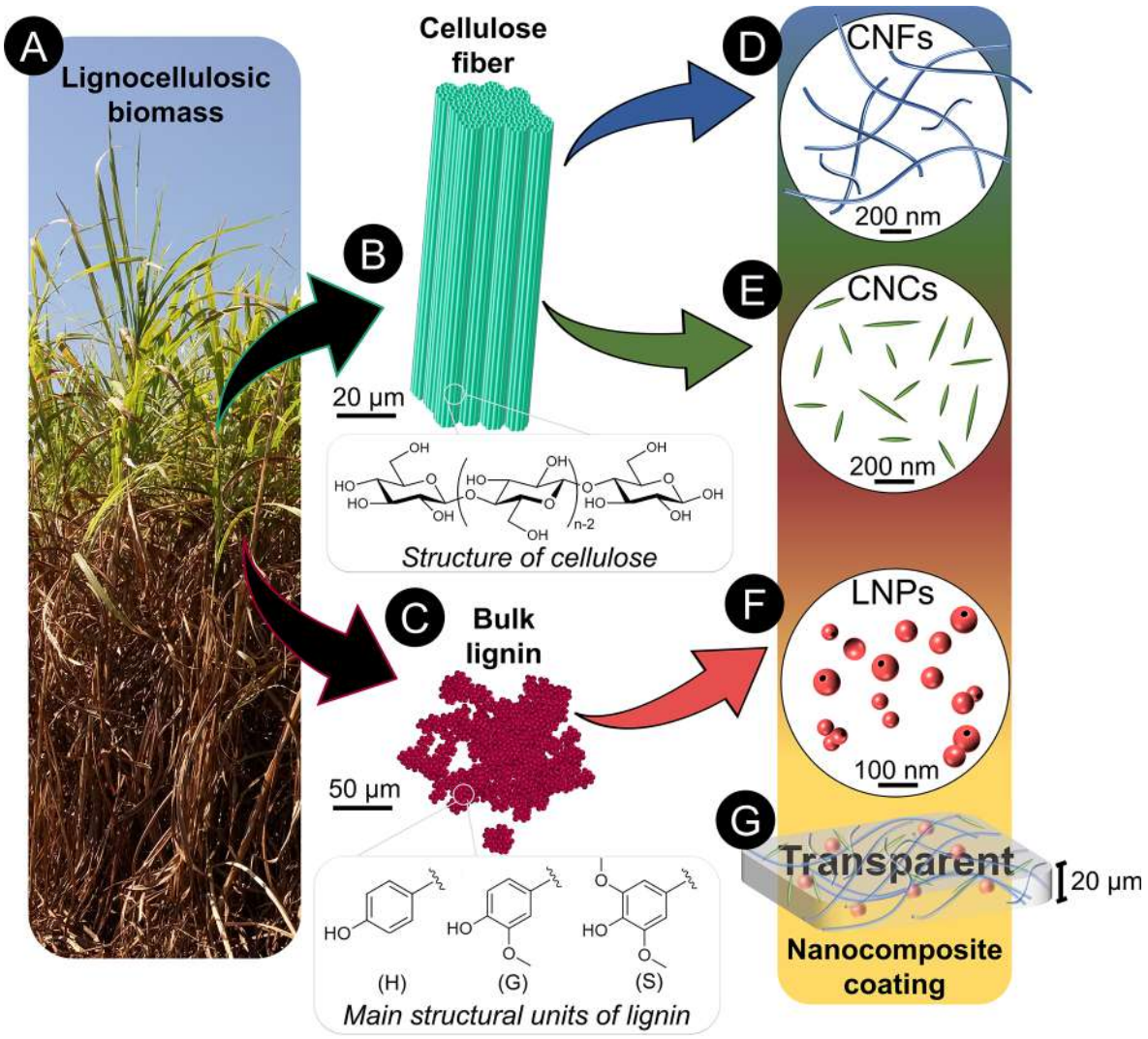

Figure 1. Depiction of the origin of cellulose and lignin and their extraction and conversion into the nanoparticles that were used to produce nanocomposite coatings. (A) Elephant grass biomass underwent a sequential two-step pretreatment with diluted H_2SO_4 and NaOH[1,2] to allow the separation and extraction of (B) cellulose fibers and (C) bulk lignin. The extracted cellulose fibers, made of cellulose chains longitudinally assembled in a hierarchical way, were converted into (D) CNFs by a TEMPO-mediated oxidation process or (E) CNCs by sulfuric acid hydrolysis. The isolated lignin, in which the main structural units are the phenylpropanoids *p*-hydroxyphenyl (H), guaiacyl (G), and syringyl (S), was solubilized in acetone and converted into (F) LNPs by the addition of excess water as an antisolvent. All nanoparticles were produced in water and mixed to result in (G) transparent nanocomposite coating films with an average thickness of *ca.* 20 μm.

and chemical properties of transparent nanocelluloses and the antioxidant and UV-blocking properties of light-colored nanolignin, coating formulations were prepared using a combination of aqueous dispersions of CNFs, CNCs, and LNPs.[36] These nanoparticles were extracted from surpluses of elephant grass biomass,[1,2] a widely available forage crop similar to sugarcane,[49] used mainly as dairy cattle feed in Brazil.[50] Figure 1 depicts a schematic of the methodologies used to produce the nanostructures and their amalgamation to form the coating systems.

CNFs presented an elongated, filament-like morphology (Figure 2A,B) with an average diameter as small as 10 nm. Leaf nanofibrils were shorter (around 600 nm long) than stem nanofibrils (1.1 μm long). Thus, leaf and stem CNFs were combined in a 2:1 ratio, forming a nanocellulosic matrix with enhanced tensile mechanical behavior, being the expected ultimate tensile strength and Young's modulus as high as 45 MPa and 2 GPa, respectively.[1] The CNF content in the dry nanocomposite coatings varied from 60 to 66 wt % (Figure 2E).

CNCs presented a typical needle, rod-like morphology (Figure 2C) with an average diameter as small as 7 nm and a length of *ca.* 130 nm.[1]. The CNC content in the dry nanocomposite coatings varied from 30 to 34 wt % (Figure 2E).

Self-assembled LNPs exhibited a spherical morphology with the occasional presence of single holes on the surface (Figure 2D). The average diameter of these nanoparticles was below 100 nm.[2] The LNP content in the nanocomposite coatings varied from 0 to 10 wt % (Figure 2E).

When combined in aqueous dispersion and cast-dried, these three nanostructures entangled to form continuous, compacted, smooth nanocellulose-based matrices with LNPs relatively well distributed throughout the films (Figure S3).

Visual Aspect of Nanocellulose/Nanolignin-Coated Cellulosic Substrates. NFC, NFCL1, and NFCL10 coating

https://doi.org/10.1021/acsanm.2c02968
ACS Appl. Nano Mater. 2022, 5, 13245−13259

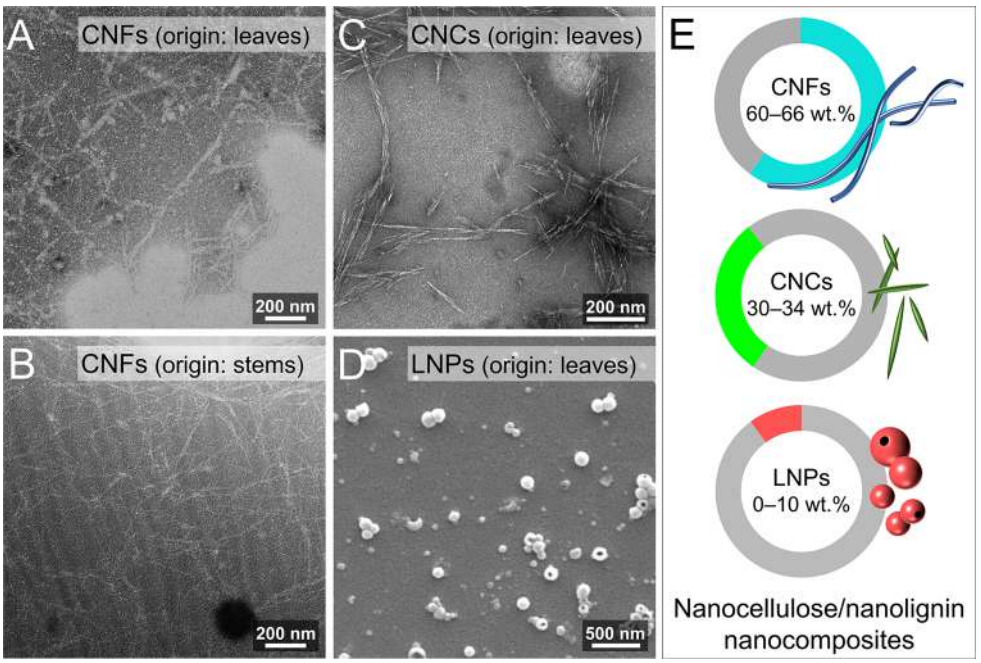

Figure 2. TEM images of nanostructures prepared using elephant grass biomass: (A) CNFs originated from leaves, (B) CNFs originated from stems, (C) CNCs originated from leaves. (D) SEM image of LNPs produced using bulk lignin isolated from grass leaves. (E) Percentage ratio and depiction of the typical morphology of each component in the formulations of nanocellulose/nanolignin nanocomposites.

formulations, containing 0, 1, and 10 wt % LNPs, respectively, as well as the acrylic resin Paraloid B72 were brush-applied on the surface of balsa wood, cotton paper, and unbleached cotton fabric. The average coating thickness on wood, paper, and fabric, respectively, was estimated to be about 22 ± 8, 20 ± 5, and 18 ± 5 μm for nanocomposites and 26 ± 7, 20 ± 4, and 19 ± 5 μm for commercial varnish (Figure S4).

As shown in the photographs inserted as details in Figure 3, the coating application did not imply any major or striking difference in the visual aspect of the substrates. The ability to preserve the aesthetic features or to modify it as little as possible is crucial in coating technologies for diverse applications, such as the protection of cultural, artistic, and/or historical artifacts.[51] Nevertheless, in paper and fabric, alterations in the surface colorimetric parameters measured in the CIEL*a*b* color space could be observed when the coated and uncoated substrates were compared.

A color difference (ΔE) higher than 2 indicates the existence of some discrepancy between the colors of two samples; i.e., a standard observer can perceive the color difference between them.[47] ΔE or the variation in coordinates L^*, a^*, and b^* were not significant for the coated wood substrate (Figure 3A). On the other hand, decreases in L^* and increases in b^*, i.e., darkening and yellowing (browning), resulted in noticeable ΔE for NFCL1- and NFCL10-coated paper but not for NFC- and Paraloid B72-coated paper (Figure 3B). In the case of fabric mockups, only the NFCL10 coating significantly changed the colorimetric parameters L^* and b^*, causing appreciable ΔE to the coated sample (Figure 3C).

Such colorimetric alterations do not preclude the widespread use of the nanocomposite coatings on the cellulosic substrates studied here. However, this behavior should be considered critically on a case-by-case basis before practical applications. Remarkably, LNP-containing coatings could be especially suitable for protecting, for example, wooden sculptures, furniture or archeological artifacts, as well as yellowed papers. In fact, a preliminary study indicated only a moderate color difference (ΔE = 3.5) when a nanocellulose coating with LNPs was applied to the surface of tinted, yellowed paper samples obtained by an artificial thermal/acid/oxidative aging protocol (Figure S5). In this case, the presence of high concentrations of yellowish/brownish degradation products imparts, from the beginning, a major contribution of darkness and yellow CIEL*a*b* coordinates to the substrates, minimizing the color changes potentially caused by the coating application.

Effect of Nanocellulose/Nanolignin-Based Coatings on the Protection of Cellulosic Substrates under Moist-Heat Aging and UV Radiation. Moist-heat aging can severely damage wood,[52] paper,[33] and fabric.[53] In fact, the variation of colorimetric parameters comparing aged and unaged samples was significant when all the uncoated substrates underwent a hydrothermal accelerated aging at 80 °C and 75% RH for 168 h (Figure S6). Consequently, ΔE was superior to 2, indicating a noticeable color difference for these samples (Figure 4A). Uncoated paper and fabric, as well as the substrates coated with Paraloid B72, presented the most dramatic color changes upon aging. The presence of nanocomposite coatings, in turn, minimized the color changes in paper and did not influence ΔE of coated wood and fabric after aging. This behavior suggested that nanocellulose/nanolignin-based coatings stabilized and protected the cellulosic surfaces against moist-heat aging. Self-standing nanocomposite films with analogous formulations exhibited an excellent colorimetric stability when aged under harsh conditions of temperature and relative humidity.[36] Furthermore, the presence of small amounts of residual lignin (<4 wt %) in CNFs and CNCs,[1] as well as the high crystallinity of CNCs and chemical stability of nanocelluloses,[36,54] likely contributed to the better aging performance of NFC-coated paper as compared to uncoated paper.

https://doi.org/10.1021/acsanm.2c02968
ACS Appl. Nano Mater. 2022, 5, 13245−13259

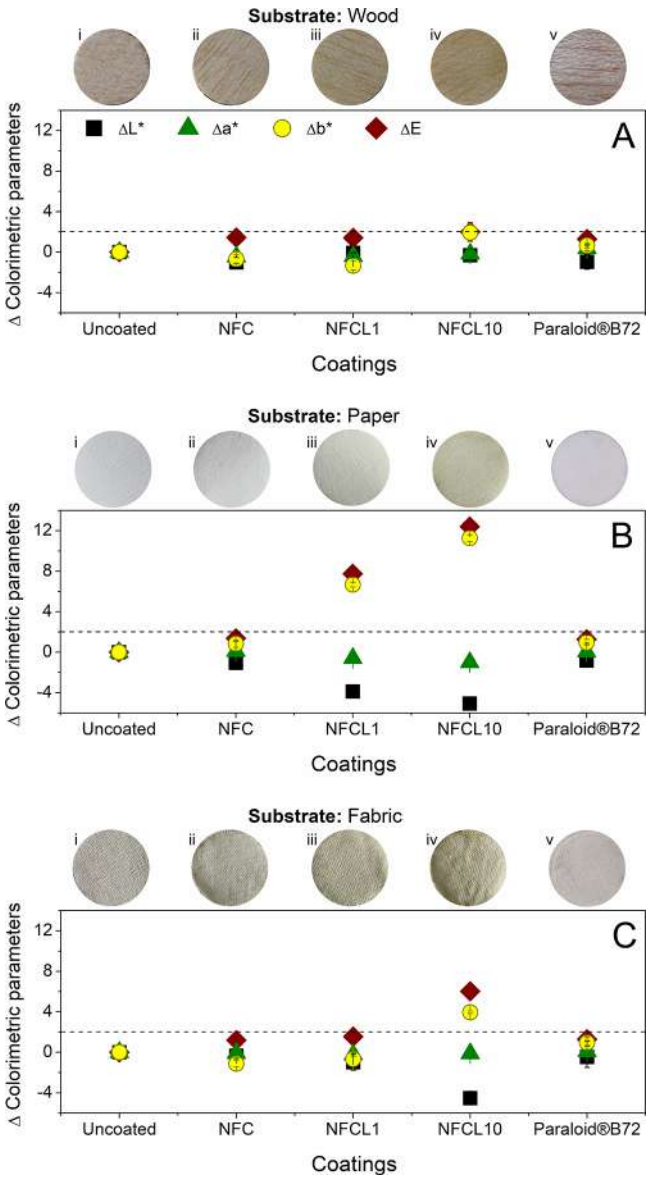

Figure 3. Variation of colorimetric parameters (ΔL^*, Δa^*, and Δb^*) and color difference (ΔE) between uncoated and coated substrates: (A) wood, (B) paper, and (C) fabric. For uncoated mockups, all variations were set to zero. Values were expressed as the average and standard deviation (error bars) of at least four replicates. The dotted lines demarcate a tolerance limit of 2 on the ordinate axis. Details inserted are photographs under visible light of (i) uncoated, (ii) NFC-coated, (iii) NFCL1-coated, (iv) NFCL10-coated, and (v) Paraloid B72-coated substrates. Some difference in ranking light can be observed between the photos.

Vardanyan et al.[55] showed that the incorporation of a low amount of CNCs (0.5 to 2 wt %) improved the efficiency of polyurethane-based synthetic varnishes in protecting the color of coated wood samples during long exposure to weathering (UVA light source, 63 °C, 50% RH, presence of water spray). The higher protection performance was attributed to the UV-light scattering promoted by the nanocrystals. Here, in addition to the presence of CNFs and a larger amount of highly crystalline CNCs, which are quite resistant to chemical attacks, the incorporation of antioxidant LNPs likely contributed to the excellent performance of the protective coatings under moist-heat conditions. Elephant grass nano-lignins dispersed in water[2] or incorporated at 1 wt % into the nanocomposite thin films[36] showed up to 80% and 40% of free radical scavenging activity, respectively. Tan et al.[56] reported lower ΔE for medium-density fiberboard (MDF) coated with varnishes based on a styrene−acrylate copolymer incorporated with 1 wt % colloidal organosolv lignin nanospheres when compared to pure varnish or commercial varnish-coated MDF during dry weathering (UVA light source, 60 °C for up to 100 h). Similarly, Zikeli et al.[14] evaluated the use of LNPs for the treatment of wooden surfaces and observed, despite the initial increase of yellowness, that LNP-based coatings mitigated the color changes, reaching lower yellowing than the uncoated wood control after accelerated dry weathering (UVA light source, 50 ° C, 20% RH for up to 7 days). The superior chromatic performance and aging resistance of LNP-based coatings and LNP-incorporated varnishes/stains, also verified by Smyth,[57] can be attributed to the long-term scavenging activity and UV protection ability (encompassing the generation of new free radicals). The durable efficiency of LNPs is likely provided by the three-dimensional crosslinked nature of the lignin macromolecule,[56] whose structure is confined in individualized nanospheres with an enlarged surface area but a discrete geometry. These colloidal particles are separated and distributed throughout the coating, unlike the native macromolecular lignin that forms a continuous network in the wood cell wall (lignocellulosic matrix), for example.

Along with moist-heat and weathering, the exposure to light radiation, particularly in the ultraviolet range, can also trigger cellulose degradation through oxidative and photo-oxidative pathways.[58] Display cases with UV-protective glazing are commonly used to shield organic artifacts from UV radiation in museums. Nevertheless, when appropriate, suitable polymeric coating films containing UV-shielding compounds can be directly applied to the object surface.[59] An intrinsically bound coating can likely ensure a more efficient UV protection, especially when the artifact must be exhibited, handled, or accessed by users. Thus, the photoabsorbance of the nanocomposite films and their capacity to protect substrates under the incidence of UV radiation were evaluated as well.

In Figure 4B, the DRS spectra evidenced that lignin-containing nanocomposite and Paraloid B72 self-standing films were able to effectively absorb the UV radiation in the range of 200−250 nm. As shown in Table S1, the nanocomposite containing 10 wt % LNPs (NFCL10) showed the highest and broadest photoabsorption efficiency, with transmittance as low as 6% in the UVA region, 2% in the UVB, and 0% in the UVC region. The commercial varnish also showed zero transmittance in the UVC region and was the most transparent in the visible range (91% transmittance at 600 nm), followed by NFC and NFCL1 self-standing films.

A UV-irradiation assay was carried out to assess the UV-blocking property of all the transparent films.[45] Paraloid B72 and nanocomposite films were overlaid onto polypropylene (PP) films, intercepting the direct incidence of a UVA/UVB light source. This is a standard assay used to evaluate the UV protection capability of overlapping films, since pristine PP contains only carbon and hydrogen atoms, making it easy to observe chemical changes due to its photo-oxidation. The ATR-FTIR spectra of control and PP samples under the films, irradiated for 24 h, indicated that no detectable chemical change occurred in the short-term exposure (Figure 4C). After 72 h, a new subtle absorption band around 1720 cm^{-1}

https://doi.org/10.1021/acsanm.2c02968
ACS Appl. Nano Mater. 2022, 5, 13245−13259

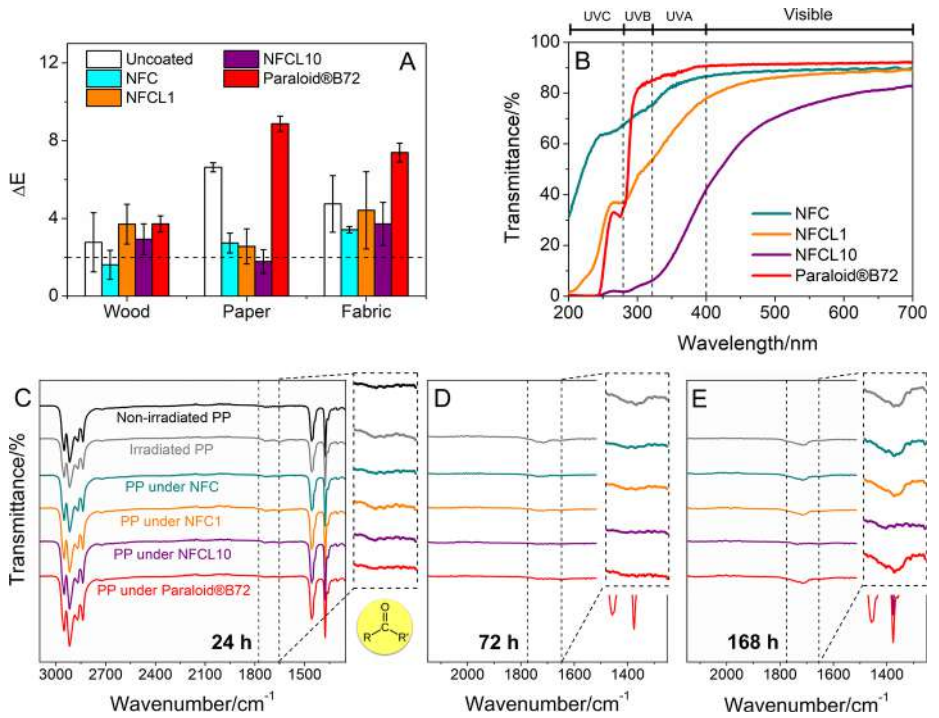

Figure 4. (A) ΔE calculated for uncoated and coated substrates after aging at 80 °C and 75% RH for 168 h in comparison to unaged uncoated and coated substrates. Values were expressed as the average and standard deviation (error bars) of at least four replicates. The dotted line demarcates a tolerance limit of 2 on the ordinate axis. (B) UV−vis DRS spectra of nanocomposite and Paraloid B72 self-standing films. ATR-FTIR spectra of PP samples subjected to a UV-irradiation assay for (C) 24 h, (D) 72 h, and (E) 168 h. The spectra labeled as irradiated and non-irradiated PP are the reference spectra (control), while the other spectra correspond to PP samples that were placed under self-standing films of nanocomposites or commercial resin. Regions delimited by the dotted lines and the inserted details indicate the adsorption band at *ca.* 1770−1650 cm^{-1}, assigned to the carbonyl functional group related to PP photo-oxidation.

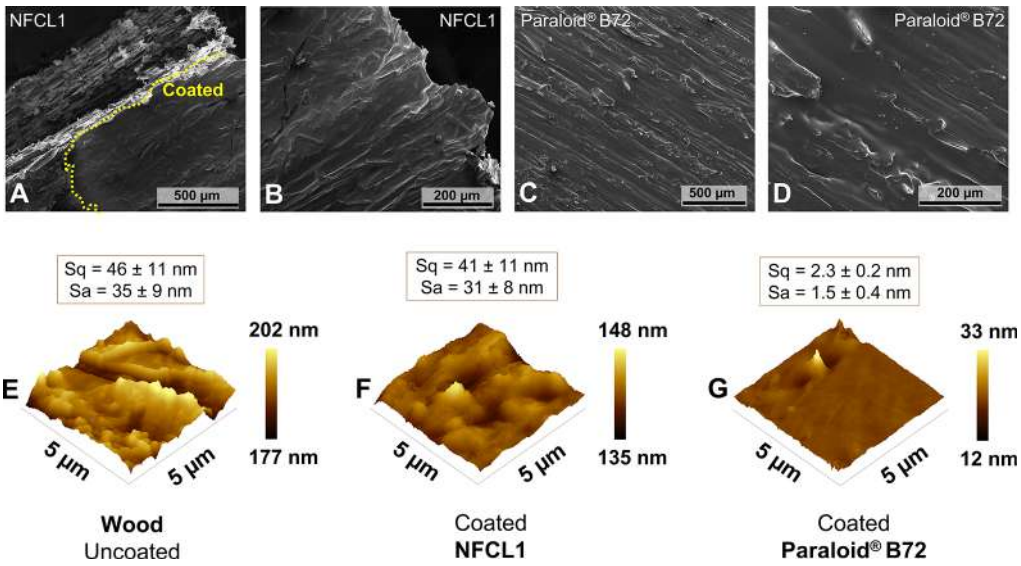

Figure 5. SEM images of the surface of the wood substrate coated with (A, B) NFCL1 nanocomposite film and (C, D) Paraloid B72 at different magnifications. The yellow dotted line in (A) indicates a boundary between coated and uncoated areas. 3D AFM topography mapping of the wood surface: (E) uncoated, (F) NFCL1-coated, and (G) Paraloid B72-coated. Dimensions: 5 × 5 μm. The tip curvature radius was less than 8 nm. The false color scales indicate the variation of heights between the maximum peak height (lighter color) and the maximum pit depth (darker color). The Sq and Sa roughness values are shown separately for each sample as the average ± standard deviation of duplicate measurements taken on different sample areas.

indicated that the control PP sample likely started to degrade under UV irradiation (Figure 4D). This absorption band was assigned to the stretching vibration of carbonyl groups,[45] attributable to PP photo-oxidation. Such a shoulder was yet absent in the spectra of other PP samples, thus suggesting that all self-standing films presented UV-shielding properties for at least 72 h. Nevertheless, after 168 h of exposure, the carbonyl band at *ca.* 1720 cm^{-1} was discernible in the spectra of all PP

https://doi.org/10.1021/acsanm.2c02968
ACS Appl. Nano Mater. 2022, 5, 13245−13259

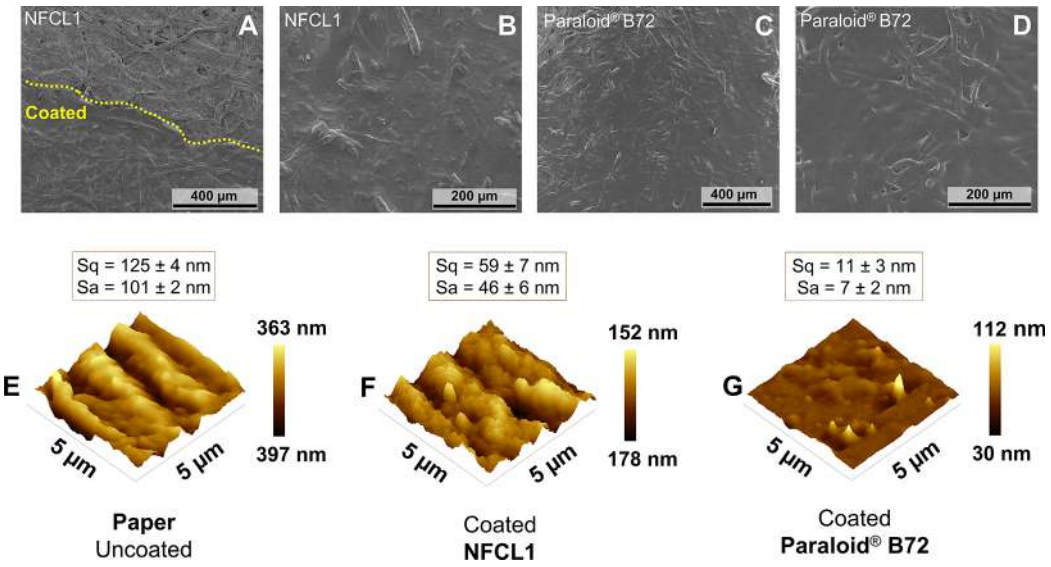

Figure 6. SEM images of the surface of the paper substrate coated with (A, B) NFCL1 nanocomposite film and (C, D) Paraloid B72 at different magnifications. The yellow dotted line in (A) indicates a boundary between coated and uncoated areas. 3D AFM topography mapping of the paper surface: (E) uncoated, (F) NFCL1-coated, and (G) Paraloid B72-coated. The Sq and Sa roughness values are shown separately for each sample as the average ± standard deviation of duplicates.

samples except that under the NFCL10 nanocomposite film (Figure 4E). No visual color change was noticed for any of the films studied after UV irradiation.

The longer-lasting UV-shielding ability of the nanocomposite containing 10 wt % LNPs can be attributed to the higher lignin content in this system, favoring its potential use as an adequately transparent UV-protective coating. Farooq et al.[3] and Parit et al.[5] used the same loading of softwood Kraft LNPs or solubilized Kraft lignin (bulk), respectively, to prepare CNF/LNP or CNC/lignin composite films rather opaque (less than 50% transmittance at 600 nm), but which were equally efficient to absorb in the range of 200−400 nm. Cusola and collaborators[8] reported a full UV-blocking effect for loadings greater than 15 wt % lignin particles in opaque CNF membranes. In addition to its antioxidant activity,[2] lignin possesses high absorption capability in the UV/visible region due to its aromatic structure, with the presence of chromophores.[60] The self-assembly of this phenolic macromolecule into nanospheres increases the confinement of $\pi-\pi$ aromatic aggregates and further enhances the UV-blocking property.[61] Hence, the incorporation of LNPs to provide both UV-shielding and antioxidant stabilization to bio-based coatings is a greener approach than the most traditional ones used in the paint and coatings industry. Conventional light stabilizers include toxic benzophenones and benzotriazoles, while widespread radical scavengers and peroxide decomposers include sterically hindered phenols and moderately toxic hydroxylamines.[62]

Effect of Nanocellulose/Nanolignin Coatings on the Surface Morphology and Roughness of Cellulosic Substrates. SEM and AFM analyses were used to assess the morphology, topography, and surface roughness of coated wood, paper, and fabric mockups.

The NFCL1 coating formed a continuous film, compatible with the micrometric texture of the wood surface (Figure 5A,B). The surface microstructure of wood fibers and veins was preserved, as well as the nanometric surface roughness (Figure 5E,F). The nanocomposite created a thin, non-penetrating, or compacting layer at the interface with the substrate. Antonelli et al.[11] also verified that CNCs, bacterial cellulose (BC), and LNPs presented low penetrability when separately applied as consolidants in waterlogged wooden objects. The commercial coating, on the other hand, filled in wood indentations, changed the surface morphology (Figure 5C,D) and decreased its roughness (Figure 5G), macroscopically causing a visual increase in brightness. The root-mean-square roughness (Sq) obtained from AFM topography images reduced from 46 nm in uncoated wood to 2 nm after the application of Paraloid B72.

The nanocomposite coating also retained the paper surface microstructure (Figure 6A,B). Even though the surface roughness decreased from *ca.* 100 nm in the uncoated to *ca.* 50 nm in the coated substrate, such reduction did not lead to pronounced surface alteration (Figure 6E,F). Paper has deep grooves as well as apparent protruding fibers on the surface. Despite filling the grooves and then decreasing the roughness, the NFCL1 coating did not agglutinate the surface fibers, maintaining its original topography. Völkel et al.[19] reported similar small alterations in the roughness of samples of historical papers consolidated with CNFs and BC. The application of Paraloid B72 again changed the surface topography, significantly decreasing the roughness (Figure 6G) and rendering a smoother surface (Figure 6C,D). Specifically for brittle and weakened paper-based artifacts, a more conventional consolidation/protection procedure than applying a copolymer coating would be lining/lamination, also called *velatura*.[63] This technique consists in introducing a thin semitransparent Japanese tissue paper as a reinforcement layer adhered on the treated paper surface, which can also impart a great visual, color, and morphological change to the coated substrate. Usually, reversible adhesives such as cellulose ethers are applied, but hot-melt or solvent-reactivated polymers can also be used.

Conversely, on the fabric substrate, Paraloid B72 penetrated in the fiber threads, stiffening warps and wefts while keeping their surface morphology mostly unchanged (Figure 7G,H)

https://doi.org/10.1021/acsanm.2c02968
ACS Appl. Nano Mater. 2022, 5, 13245−13259

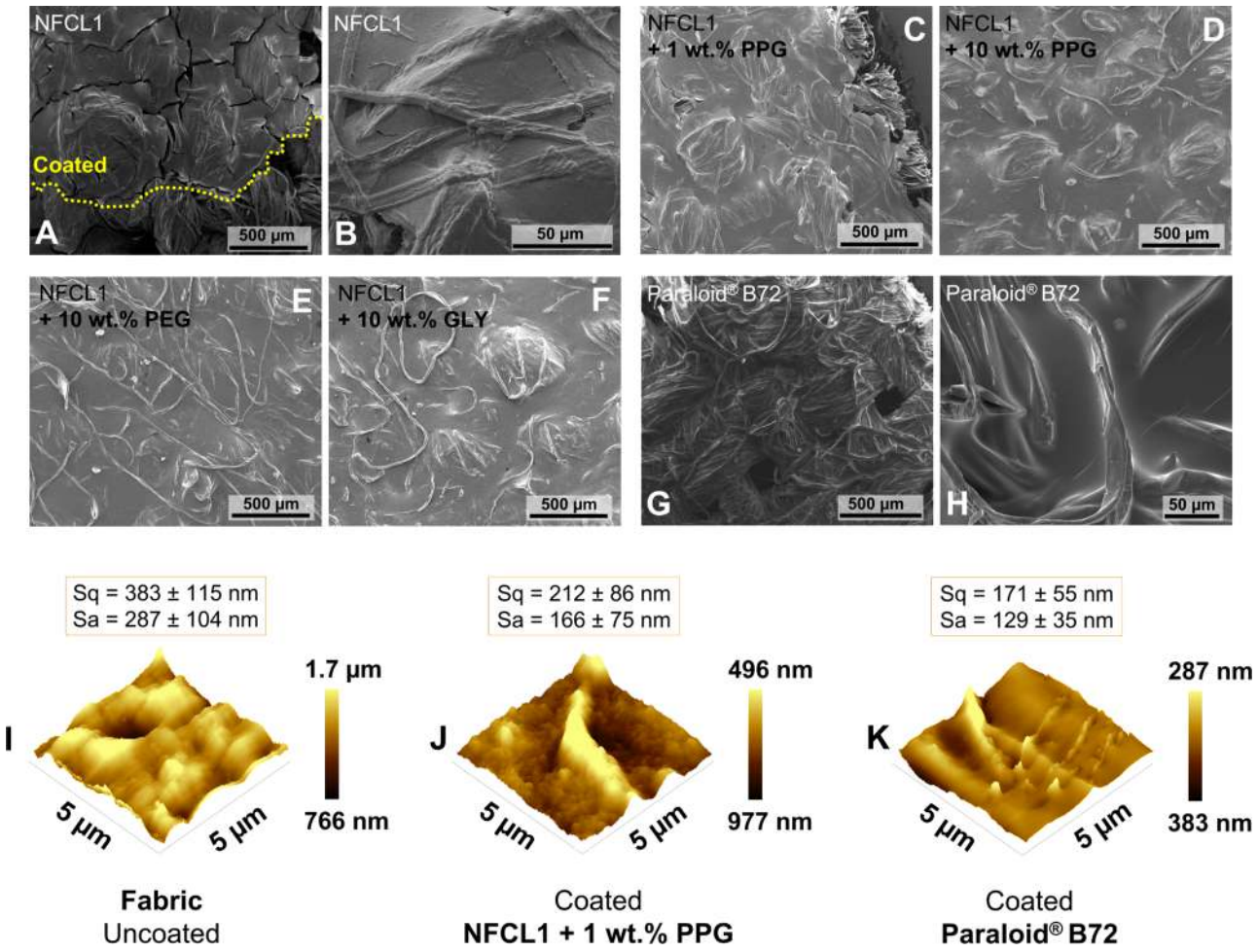

Figure 7. SEM images of the surface of the fabric substrate coated with (A, B) NFCL1 nanocomposite film, (C) NFCL1 with an addition of 1 wt % PPG, (D) NFCL1 with an addition of 10 wt % PPG, (E) NFCL1 with an addition of 10 wt % PEG, (F) NFCL1 with an addition of 10 wt % GLY, and (G, H) Paraloid B72. The yellow dotted line in (A) indicates a boundary between coated and uncoated areas. 3D AFM height mapping of the fabric surface: (I) uncoated, (J) coated with the NFCL1 nanocomposite with an addition of 1 wt % PPG 1, and (K) Paraloid B72-coated. The Sq and Sa roughness values are shown separately for each sample as the average ± standard deviation of duplicates.

and slightly reducing the original roughness (Figure 7I,K). Notwithstanding that similar behavior was verified to NFCL1, the coating layers presented flaws and cracks (Figure 7A,B). The widespread defects were likely attributed to the great malleability of raw fabric mockups. The nanocomposite did not penetrate the fabric fibers, just as coatings of CNFs or CNCs used to consolidate painting canvases.[23] Consequently, the film adhered to the fabric surface was prone to breakage during handling of the substrate.

As shown in Figure 7C−F and Figure S7, the addition of plasticizers allowed the formation of more continuous and less defective nanocomposite coatings on the fabric surface. Analogous to Paraloid B72, the nanocomposite coating containing 1 wt % PPG (Figure 7C) preserved the surface morphological profile, even though slightly reducing the original roughness of the fabric (Figure 7I,J). Polyols are plasticizers commonly used to improve deformation and flexibility of polysaccharide films.[64] More than increasing the mobility of polymer chains, in the case of the nanocellulosic matrix, using an adequate concentration of plasticizers could enhance the percolation and intermolecular interactions between nanostructures. Therefore, incorporating polyols into the nanocomposite formulation can ensure suitable coating flexibility for applications on pliable substrates. The good interaction between highly compatible plasticizers and the nanocellulosic matrix is expected to result in negligible plasticizer migration rates.[65] Nevertheless, further investigation should be conducted on the aging performance of plasticizer-incorporated nanocomposites.

Effect of Nanocellulose/Nanolignin Coatings on the Barrier Properties and Wettability of Cellulosic Substrates. Owing to cellulose hydrophilicity,[66] NFC, NFCL1, and NFCL10 nanocomposite films presented apparent water contact angles (WCA) of 36 ± 4°, 64 ± 2°, and 68 ± 3°, respectively (Figure 8A−C). These results indicate an increased hydrophobic character in the samples containing nanolignin. Wu et al.[67] and Ni et al.[68] recently reported the hydrophobization of polyurethane and starch films, respectively, with the incorporation of 1 wt % self-assembled LNPs from wheat straw and bamboo biomass. The WCA of polyurethane increased from 65° to 102°,[67] while the WCA of starch increased from 65° to 98°.[68] On the other hand, Lizundia et al.[69] observed only a slight increase in the WCA of poly(L-lactide) incorporated with LNPs from commercial alkali lignin (68° to about 71°). Analogously, thin films of self-

https://doi.org/10.1021/acsanm.2c02968
ACS Appl. Nano Mater. 2022, 5, 13245−13259

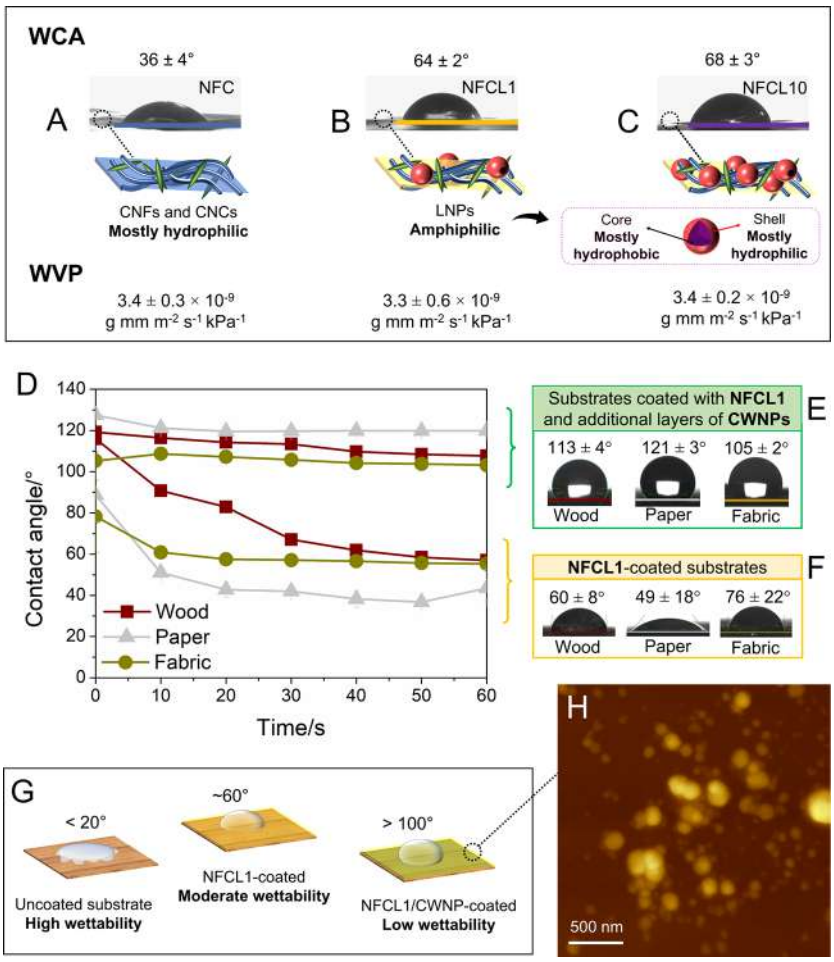

Figure 8. Average WCA and WVP results for the (A) NFC, (B) NFCL1, and (C) NFCL10 self-standing films, accompanied by the photo of the water droplet 30 s after it was deposited on the film surface and schematic depictions of the nanostructures that make up each film. Values were expressed as the average ± standard deviation of five replicates for WCA and triplicates for WVP. (D) Graph of the apparent WCA as a function of time for nanocomposite-coated substrates. The error bars are included in the markers. Average WCA and photographs of water droplets 30 s after it was deposited on wood, paper, and fabric mockups coated with (E) NFCL1 including additional layers of carnauba wax nanoparticles (CWNPs) and (F) NFCL1. (G) Schematic depiction of wettability modulation on uncoated, nanocomposite-coated, and nanocomposite-CWNP-coated substrates. (H) AFM topography image of the CWNPs.

assembled LNPs from softwood lignin presented a WCA of *ca.* 30°.[70]

Even though the native lignin is highly hydrophobic, the extracted lignin contains amphiphilic properties.[71] In water, the macromolecules self-assemble into LNPs with most of the hydrophobic moieties within the core and hydrophilic groups exposed toward the outer shell[2] (Figure 8C). Thus, the incorporation of 1 and 10 wt % LNPs minimized the nanocomposite wettability but did not impart any difference in the high water vapor permeability (WVP) of nanocelluloses.

Moisture exchange and WVP are important properties of several materials, since changes in the permeability and capillarity can cause long-term degradation and irreversible physical−mechanical damages,[72] including in cellulose-based artifacts. Single-component CNF, CNC, and nanocomposite self-standing films displayed an average WVP of *ca.* 3.5×10^{-9} g mm m^{-2} s^{-1} kPa^{-1} (Figure S8), which is within the range of WVP previously reported for CNF films[73] or wood varnishes[74] (10^{-9} to 10^{-6} g mm m^{-2} s^{-1} kPa^{-1}). The WVP of Paraloid B72 (1.9×10^{-9} g mm m^{-2} s^{-1} kPa^{-1}[74]) was smaller, although in the same order of magnitude as the WVP of nanocomposite films. On the other hand, wood, paper, and fabric mockups, being porous materials, presented WVP superior to the WVP of compact self-standing films, so that the application of thin coatings onto these substrates did not impart any change on the WVP of these mainly hydrophilic substrates (Figure S9).

In fact, the great wettability of wood and paper did not allow time-dependent WCA measurements to be performed for uncoated samples, which showed an initial WCA of about 30−50° immediately after water drop deposition. In turn, the average WCA of cotton fabric was measured as 67 ± 11° (Figure S10). Analogous to the minor influence of the coatings on the substrate WVP, NFCL1-coated substrates also presented a moderate wettability, although exhibiting a more stable WCA of less than about 76° (Figure 8D,F). Notwithstanding that WCA measurements do not elucidate holistically the dynamic behavior of the direct contact with moisture, especially considering intrinsic capillary effects, this technique allowed a qualitative assessment of the wettability of cellulosic surfaces. The results provided information about the water droplet absorption/repellency behavior and the stability of the WCA on coated surfaces.

Reduced wettability can favor the protection of restored artifacts[75] or packaging materials based on cellulose. The

https://doi.org/10.1021/acsanm.2c02968
ACS Appl. Nano Mater. 2022, 5, 13245−13259

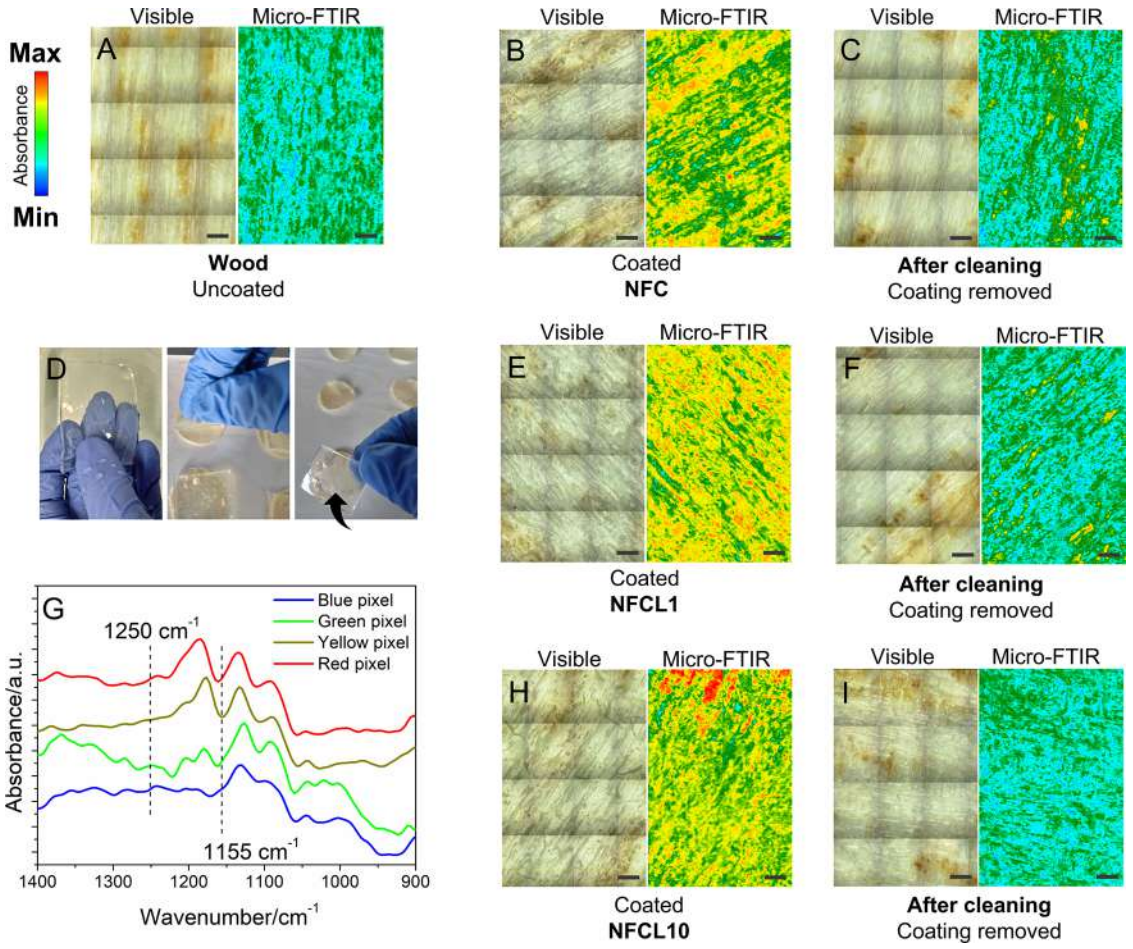

Figure 9. Optical micrographs under visible light and micro-FTIR maps for wood samples: (A) uncoated, (B, E, H) coated with nanocomposites, and (C, F, I) after cleaning/coating removal using the pHEMA/PVP hydrogel. Scale bars: 200 μm. False color scale: lowest intensity of the integrated band (1250−1155 cm^{-1}) in blue and highest intensity in red. (D) Photographs of the chemical hydrogel soaked in water and the cleaning process of the coated substrates, culminating in the removal of the coating indicated by the black arrow. (G) FTIR spectra corresponding to a representative blue, green, yellow, and red pixel. The spatial resolution of the equipment is 5.5 μm; i.e., each pixel corresponds to a sample area of about 30 μm^2.

occurrence of a more hydrophobic surface layer can minimize the interaction between water-sensitive substrates and excess humidity loading or moisture leakage. Such a feature was observed for Paraloid B72-coated wood, paper, and fabric mockups, which presented an average WCA higher than 100° (Figure S11). To improve the hydrophobicity and modulate the wettability of the nanocomposite material, additional particulate layers of CWNPs were added on top of the coating surface (Figure 8G).

A melting-dispersion technique was applied to convert carnauba wax pellets into CWNPs in aqueous dispersion (Figure S12). As confirmed by AFM topography images, these nanoparticles showed a quasi-spherical morphology (Figure 8H) and an average diameter of 246 ± 99 nm (Figure S13). CWNPs presented a zeta potential of −52 ± 9 mV, indicating a sufficient electrostatic stabilization in water due to the presence of a negatively charged surface. Besides its fatty composition, the wax is rich in hydroxyl, carboxylic acid, and aldehyde functional groups.[38] The dispersion of CWNPs was brush-applied onto the NFCL1 coating surface, resulting in whitish/semitransparent particulate layers (Figure S14) that are not expected to hinder the breathability of the nanocomposite coating or the substrate beneath it. The average WCA increased to 113° on wood, 121° on paper, and 105° on fabric substrates (Figure 8D,E). This decrease in the wettability of the coatings can be attributed to the more hydrophobic character of the wax layers after drying, even at room temperature. Thermal annealing/curing, commonly performed for carnauba wax particles applied on all-cellulose composites,[76] fabric,[77] and wood coatings,[38] was avoided here as heating can trigger the degradation of cellulosic substrates.

Regarding the use of waxes to coat paper, Jeong et al.[78] elucidated the detrimental effect of beeswax coatings applied to Korean traditional handmade paper in the early 15th century. The exclusively hydrolytic damage was attributed to the action of cellulolytic enzymes released by microorganisms feeding on the beeswax.[78] Beeswax and carnauba wax present intrinsic differences in origin (animal origin for the former and plant origin for the latter), chemical composition, and production methodology. Despite such differences, it is reasonable to consider that microorganism contamination could also be a problem in carnauba wax-based coatings. However, potential deleterious effects on the coated cellulosic substrates would likely be prevented by the existence of an intermediate nanocomposite layer between the top particulate layer of CWNPs and the wood, paper, or fabric surfaces. Regardless, maintaining proper environmental conditions during storage of the coated artifacts would be essential to hamper the

https://doi.org/10.1021/acsanm.2c02968
ACS Appl. Nano Mater. 2022, 5, 13245−13259

proliferation of biological contaminants. Future investigations into the artificial aging of CWNP-coated films and extensive natural aging of the developed coating systems, as well as their application to coat more complex mockups, would be of paramount importance to ascertain the feasibility and permanence of the introduced methodology.

Reversibility and Removal of Nanocellulose/Nanolignin Coatings Applied on Cellulosic Substrates. The compatibility, durability, and reversibility of treatments are crucial criteria in the field of conservation of cultural heritage.[51,79] While the durability of the nanocomposite coatings was confirmed by artificial aging tests, their compatibility and reversibility were further investigated by 2D micro-FTIR mapping.

Nanocelluloses/nanolignin nanocomposites are naturally and intrinsically compatible with wood, paper, and cellulosic fabric substrates. They share a unique main origin: lignocellulosic biomasses from plants. Despite the shared chemical nature, the coating layer could be distinguished and mapped by 2D micro-FTIR due to subtle variations in the chemical composition and refractive index of the sampled areas. By collecting the spectra of uncoated and coated mockups, different distributions of relative intensity of the integrated band at 1250−1155 cm^{-1} were verified (Figure 9G). The presence of nanocomposite coatings increased the intensity of such an absorption band (Figure 9B,E,H) comparatively to the mapping of uncoated wood (Figure 9A). The integrated bands could be assigned to cellulose asymmetric C−O−C stretching[80] in nanocelluloses, as well as to aryl C−O stretching mode[81] and aromatic C−H[82] in-plane deformation of guaiacyl units in LNPs.

The integrated band was then used to evaluate the reversibility of the treatment. In this context, a procedure is reversible or retractable when the materials applied can be removed, ideally requiring no solvent or the same solvent used during the application step.[83] Thus, the treated artifact can return to its state previous to the treatment and, when necessary, undergo another upgraded treatment.[51,79] Owing to their great compatibility and interaction, protective coatings and substrates adhered favorably and could not be removed simply using mechanical cleaning, i.e., abrasive methods to loosen the coating layer. Therefore, a pHEMA/PVP chemical hydrogel[48] was applied to assess the removal of the coating layer using water (Figure 9D).

After a 2 h cleaning procedure, i.e., direct contact between the water-loaded hydrogel and the surface of coated substrates, micro-FTIR mapping indicated the efficient removal of the coating layer. The relative intensity of the integrated band at 1250−1155 cm^{-1}, assigned to the presence of the nanocomposite coating, decreased over the entire sampled area of the cleaned wood substrate (Figure 9C,F,I). Similar results were also achieved while mapping uncoated, coated, and cleaned paper (Figure S15) and fabric (Figure S16).

CONCLUSIONS

Taking advantage of their different nanoscale features, different morphologies, and advanced properties, cellulose nanofibrils, cellulose nanocrystals, and lignin nanoparticles were combined in aqueous dispersions and applied as protective coatings onto cellulosic substrates, i.e., wood, paper, and fabric mockups. This novel conservation approach was built upon the intrinsic compatibility, stability, and renewability of nanocelluloses and nanolignins. These nanocomposite coatings, especially the formulations containing antioxidant LNPs, were effective to protect or mitigate the deterioration of coated substrates against moist-heat aging and presented UV-blocking properties. Surface morphology and roughness, as well as substrate vapor permeability, were mainly preserved after the coating application. Nevertheless, nanocomposite-coated hydrophilic substrates showed a more controlled wettability. Tailored hydrophobicity with water contact angles of up to 120° was achieved by applying additional particulate layers of green carnauba wax nanoparticles on top of the coating surface. In addition to their high durability, protective performance, and interfacial compatibility, the nanocellulose/nanolignin coatings are reversible treatments. Therefore, such nanocomposites are a promising green tool for the conservation of cultural heritage objects, particularly non-water-sensitive wood, paper, and textile artifacts, and can also be explored and refined as a potential protection strategy for diverse industries such as packaging, printing, textiles, and furniture. Finally, cross-cutting research on the artificial and natural aging, as well as tests on complex mockups and simulated artifacts, should be encouraged to allow further understanding of the long-term applicability of the novel coatings.

ASSOCIATED CONTENT

Supporting Information

The Supporting Information is available free of charge at https://pubs.acs.org/doi/10.1021/acsanm.2c02968.

Data of self-standing film transmittance at different wavelengths; scheme of a UV-irradiation assay; scheme and detailed description of a WVP assay; SEM images of nanocomposite films; measurements of coating average thickness; colorimetric parameters of aged/yellowed paper before and after the coating application; variation of the colorimetric parameters for uncoated and coated substrates after moist-heat aging; SEM micrographs of fabric coated with nanocomposites containing different plasticizers; graph of WVP and WVTR for self-standing films; graph of WVP for uncoated and coated substrates; photos of water droplets on the surface of uncoated cellulosic substrates and apparent WCA; graph of the WCA for Paraloid B72-coated substrates and photos of the water droplets; photos of carnauba wax pellets and CWNP dispersion; AFM micrograph and histogram of diameter distribution for CWNPs; photos of mockups coated with nanocomposite and additional layers of CWNPs; and micro-FTIR characterization of uncoated, coated, and cleaned paper and fabric mockups (PDF)

AUTHOR INFORMATION

Corresponding Author

Camila A. Rezende − *Physical Chemistry Department, Institute of Chemistry, University of Campinas − UNICAMP, Campinas, SP 13083-970, Brazil;* orcid.org/0000-0002-2072-1361; Phone: +55-19-35212104; Email: camilaiq@unicamp.br

Authors

Camilla H. M. Camargos − *Physical Chemistry Department, Institute of Chemistry, University of Campinas − UNICAMP, Campinas, SP 13083-970, Brazil; CSGI and Chemistry Department, University of Florence, Sesto*

Fiorentino, FI 50019, Italy; orcid.org/0000-0002-5240-036X

Giovanna Poggi − *CSGI and Chemistry Department, University of Florence, Sesto Fiorentino, FI 50019, Italy;* orcid.org/0000-0002-4158-0705

David Chelazzi − *CSGI and Chemistry Department, University of Florence, Sesto Fiorentino, FI 50019, Italy;* orcid.org/0000-0001-9994-3356

Piero Baglioni − *CSGI and Chemistry Department, University of Florence, Sesto Fiorentino, FI 50019, Italy;* orcid.org/0000-0003-1312-8700

Complete contact information is available at: https://pubs.acs.org/10.1021/acsanm.2c02968

Notes

The authors declare no competing financial interest.

■ ACKNOWLEDGMENTS

We acknowledge IQ-UNICAMP and CSGI-UniFI for providing infrastructure and access to analysis equipment and Dr. Douglas Soares (*in memoriam*) and INCT-INOMAT for providing access to the TEM and AFM facilities. We thank Felipe Meneses for the preliminary data on artificially aged paper. We would also like to thank the LME/LNNano/CNPEM for the technical support during the electron microscopy work. Financial support was granted by the São Paulo Research Foundation (FAPESP, grant 2018/23769-1), the National Council for Scientific and Technological Development (CNPq, grants 140558/2017-9 and 420031/2018-9), Coordenação de Aperfeiçoamento de Pessoal de Nível Superior (Brazil) (CAPES, financial code 001), and Ministero degli Affari Esteri e della Cooperazione Internazionale (Italy).

■ REFERENCES

(1) Camargos, C. H. M.; Rezende, C. A. Structure-Property Relationships of Cellulose Nanocrystals and Nanofibrils: Implications for the Design and Performance of Nanocomposites and All-Nanocellulose Systems. *ACS Appl. Nano Mater.* **2021**, *4*, 10505−10518.

(2) Camargos, C. H. M.; Rezende, C. A. Antisolvent versus Ultrasonication: Bottom-up and Top-down Approaches to Produce Lignin Nanoparticles (LNPs) with Tailored Properties. *Int. J. Biol. Macromol.* **2021**, *193*, 647−660.

(3) Farooq, M.; Zou, T.; Riviere, G.; Sipponen, M. H.; Österberg, M. Strong, Ductile, and Waterproof Cellulose Nanofibril Composite Films with Colloidal Lignin Particles. *Biomacromolecules* **2019**, *20*, 693−704.

(4) Poggi, G.; Chelazzi, D.; Laurati, M. Mechanical Response and Yielding Transition of Silk-Fibroin and Silk-Fibroin/Cellulose Nanocrystals Composite Gels. *Colloids Surf., A* **2022**, *636*, 128121.

(5) Parit, M.; Saha, P.; Davis, V. A.; Jiang, Z. Transparent and Homogenous Cellulose Nanocrystal/Lignin UV-Protection Films. *ACS Omega* **2018**, *3*, 10679−10691.

(6) Österberg, M.; Vartiainen, J.; Lucenius, J.; Hippi, U.; Seppälä, J.; Serimaa, R.; Laine, J. A Fast Method to Produce Strong NFC Films as a Platform for Barrier and Functional Materials. *ACS Appl. Mater. Interfaces* **2013**, *5*, 4640−4647.

(7) Otoni, C. G.; Figueiredo, J. S. L.; Capeletti, L. B.; Cardoso, M. B.; Bernardes, J. S.; Loh, W. Tailoring the Antimicrobial Response of Cationic Nanocellulose-Based Foams through Cryo-Templating. *ACS Appl. Bio Mater.* **2019**, *2*, 1975−1986.

(8) Cusola, O.; Rojas, O. J.; Roncero, M. B. Lignin Particles for Multifunctional Membranes, Antioxidative Microfiltration, Patterning, and 3D Structuring. *ACS Appl. Mater. Interfaces* **2019**, *11*, 45226−45236.

(9) Yang, W.; Owczarek, J. S.; Fortunati, E.; Kozanecki, M.; Mazzaglia, A.; Balestra, G. M.; Kenny, J. M.; Torre, L.; Puglia, D. Antioxidant and Antibacterial Lignin Nanoparticles in Polyvinyl Alcohol/Chitosan Films for Active Packaging. *Ind. Crops Prod.* **2016**, *94*, 800−811.

(10) Hamed, S. A. A. K. M.; Hassan, M. L. A New Mixture of Hydroxypropyl Cellulose and Nanocellulose for Wood Consolidation. *J. Cult. Heritage* **2019**, *35*, 140−144.

(11) Antonelli, F.; Galotta, G.; Sidoti, G.; Zikeli, F.; Nisi, R.; Davidde Petriaggi, B.; Romagnoli, M. Cellulose and Lignin Nano-Scale Consolidants for Waterlogged Archaeological Wood. *Front. Chem.* **2020**, *8*, 32.

(12) Veigel, S.; Grüll, G.; Pinkl, S.; Obersriebnig, M.; Müller, U.; Gindl-Altmutter, W. Improving the Mechanical Resistance of Waterborne Wood Coatings by Adding Cellulose Nanofibres. *React. Funct. Polym.* **2014**, *85*, 214−220.

(13) Kluge, M.; Veigel, S.; Pinkl, S.; Henniges, U.; Zollfrank, C.; Rössler, A.; Gindl-Altmutter, W. Nanocellulosic Fillers for Waterborne Wood Coatings: Reinforcement Effect on Free-Standing Coating Films. *Wood Sci. Technol.* **2017**, *51*, 601−613.

(14) Zikeli, F.; Vinciguerra, V.; D'Annibale, A.; Capitani, D.; Romagnoli, M.; Scarascia Mugnozza, G. Preparation of Lignin Nanoparticles from Wood Waste for Wood Surface Treatment. *Nanomaterials* **2019**, *9*, 281.

(15) Xu, Q.; Poggi, G.; Resta, C.; Baglioni, M.; Baglioni, P. Grafted Nanocellulose and Alkaline Nanoparticles for the Strengthening and Deacidification of Cellulosic Artworks. *J. Colloid Interface Sci.* **2020**, *576*, 147−157.

(16) Camargos, C. H. M.; Figueiredo, J. C. D.; Pereira, F. V. Cellulose Nanocrystal-Based Composite for Restoration of Lacunae on Damaged Documents and Artworks on Paper. *J. Cult. Heritage* **2017**, *23*, 170−175.

(17) Camargos, C. H. M.; Figueiredo, J. C. D.; Pereira, F. V. Nanocellulose for Conservation and Restoration of Graphic Documents. In *Experience and Evidence: ICOM-CC Graphic Documents Working Group, Interim Meeting*; French National Library: Paris, 2016; p 14.

(18) Operamolla, A.; Mazzuca, C.; Capodieci, L.; Di Benedetto, F.; Severini, L.; Titubante, M.; Martinelli, A.; Castelvetro, V.; Micheli, L. Toward a Reversible Consolidation of Paper Materials Using Cellulose Nanocrystals. *ACS Appl. Mater. Interfaces* **2021**, *13*, 44972−44982.

(19) Völkel, L.; Ahn, K.; Hähner, U.; Gindl-Altmutter, W.; Potthast, A. Nano Meets the Sheet: Adhesive-Free Application of Nanocellulosic Suspensions in Paper Conservation. *Heritage Sci.* **2017**, *5*, 23.

(20) Dreyfuss-Deseigne, R. Nanocellulose Films in Art Conservation. *J. Pap. Conserv.* **2017**, *18*, 18−29.

(21) Puceković, N.; Hooimeijer, A.; Lozo, B. Cellulose Nanocrystals Coating − A Novel Paper Coating for Use in the Graphic Industry. *Acta Graph. - Znan. Časopis za Tisk. i Graf. Komun.* **2015**, *26*, 21−26.

(22) Jia, M.; Zhang, X.; Weng, J.; Zhang, J.; Zhang, M. Protective Coating of Paper Works : ZnO / Cellulose Nanocrystal Composites and Analytical Characterization. *J. Cult. Heritage* **2019**, *38*, 64−74.

(23) Nechyporchuk, O.; Kolman, K.; Bridarolli, A.; Odlyha, M.; Bozec, L.; Oriola, M.; Campo-Francés, G.; Persson, M.; Holmberg, K.; Bordes, R. On the Potential of Using Nanocellulose for Consolidation of Painting Canvases. *Carbohydr. Polym.* **2018**, *194*, 161−169.

(24) Kolman, K.; Nechyporchuk, O.; Persson, M.; Holmberg, K.; Bordes, R. Combined Nanocellulose/Nanosilica Approach for Multiscale Consolidation of Painting Canvases. *ACS Appl. Nano Mater.* **2018**, *1*, 2036−2040.

(25) Zimniewska, M.; Kozłowski, R.; Batog, J. Nanolignin Modified Linen Fabric as a Multifunctional Product. *Mol. Cryst. Liq. Cryst.* **2008**, *484*, 43−50.

(26) Cianci, C.; Chelazzi, D.; Poggi, G.; Modi, F.; Giorgi, R.; Laurati, M. Hybrid Fibroin-Nanocellulose Composites for the Consolidation of Aged and Historical Silk. *Colloids Surf., A* **2022**, *634*, 127944.
(27) Fortunati, E.; Verma, D.; Luzi, F.; Mazzaglia, A.; Torre, L.; Balestra, G. M. Novel Nanoscaled Materials from Lignocellulosic Sources: Potential Applications in the Agricultural Sector. In *Handbook of Ecomaterials*; Springer International Publishing: Cham, 2017; pp. 1−24, DOI: 10.1007/978-3-319-48281-1_15-1.
(28) Glasser, W. G. About Making Lignin Great Again—Some Lessons From the Past. *Front. Chem.* **2019**, *7*, 565.
(29) Sadeghifar, H.; Venditti, R.; Jur, J.; Gorga, R. E.; Pawlak, J. J. Cellulose-Lignin Biodegradable and Flexible UV Protection Film. *ACS Sustainable Chem. Eng.* **2017**, *5*, 625−631.
(30) Hölling, H. The Technique of Conservation: On Realms of Theory and Cultures of Practice. *J. Inst. Conserv.* **2017**, *40*, 87−96.
(31) Brandi, C. *Teoria Da Restauração*; Ateliê Editorial: Cotia, 2008.
(32) Fellers, C.; Iversen, T.; Lindstrom, T.; Nilsson, T.; Rigdahl, M. *Ageing/Degradation of Paper, a Literature Survey*; 1989.
(33) Małachowska, E.; Dubowik, M.; Boruszewski, P.; Łojewska, J.; Przybysz, P. Influence of Lignin Content in Cellulose Pulp on Paper Durability. *Sci. Rep.* **2020**, *10*, 19998.
(34) Schmidt, J. A.; Rye, C. S.; Gurnagul, N. Lignin Inhibits Autoxidative Degradation of Cellulose. *Polym. Degrad. Stab.* **1995**, *49*, 291−297.
(35) Vänskä, E.; Vihelä, T.; Peresin, M. S.; Vartiainen, J.; Hummel, M.; Vuorinen, T. Residual Lignin Inhibits Thermal Degradation of Cellulosic Fiber Sheets. *Cellulose* **2016**, *23*, 199−212.
(36) Camargos, C. H. M.; Poggi, G.; Chelazzi, D.; Baglioni, P.; Rezende, C. A. Strategies to Mitigate the Synergistic Effects of Moist-Heat Aging on TEMPO-Oxidized Nanocellulose. *Polym. Degrad. Stab.* **2022**, *200*, 109943.
(37) Boelsums, M.; de Figueiredo Junior, J. C. D.; Cruz Souza, L. A. Low Toxicity Solvent Compositions for Varnishes Formulations for Use in Art Conservation. *Conservar Patrimonio* **2020**, DOI: 10.14568/cp2020041.
(38) Lozhechnikova, A.; Bellanger, H.; Michen, B.; Burgert, I.; Österberg, M. Surfactant-Free Carnauba Wax Dispersion and Its Use for Layer-by-Layer Assembled Protective Surface Coatings on Wood. *Appl. Surf. Sci.* **2017**, *396*, 1273−1281.
(39) Vinçotte, A.; Beauvoit, E.; Boyard, N.; Guilminot, E. Effect of Solvent on PARALOID® B72 and B44 Acrylic Resins Used as Adhesives in Conservation. *Herit. Sci.* **2019**, *7*, 42.
(40) Pataki, A. Remoistenable Tissue Preparation and Its Practical Aspects. *Restaurator* **2009**, *30*, 51−69.
(41) Cappitelli, F.; Zanardini, E.; Sorlini, C. The Biodeterioration of Synthetic Resins Used in Conservation. *Macromol. Biosci.* **2004**, *4*, 399−406.
(42) Cappitelli, F.; Sorlini, C.; Pedemonte, E.; Princi, E.; Vicini, S. Effectiveness of Graft Synthetic Polymers in Preventing Biodeterioration of Cellulose-Based Materials. *Macromol. Symp.* **2006**, *238*, 84−91.
(43) Zervos, S.; Moropoulou, A. Cotton Cellulose Ageing in Sealed Vessels. Kinetic Model of Autocatalytic Depolymerization. *Cellulose* **2005**, *12*, 485−496.
(44) Forney, C. F.; Brandl, D. G. Control of Humidity in Small Controlled-Environment Chambers Using Glycerol-Water Solutions. *HortTechnology* **1992**, *2*, 52−54.
(45) Feng, Y.; Zhang, J.; He, J.; Zhang, J. Transparent Cellulose/Polyhedral Oligomeric Silsesquioxane Nanocomposites with Enhanced UV-Shielding Properties. *Carbohydr. Polym.* **2016**, *147*, 171−177.
(46) ASTM *E96-00: Standard Test Methods for Water Vapor Transmission of Materials*; ASTM: West Conshohocken, 2002.
(47) Mokrzycki, W. S.; Tatol, M. Colour Difference ΔE - A Survey. *Mach. Graphics Vision* **2011**, *20*, 383−411.
(48) Baglioni, M.; Domingues, J. A. L.; Carretti, E.; Fratini, E.; Chelazzi, D.; Giorgi, R.; Baglioni, P. Complex Fluids Confined into Semi-Interpenetrated Chemical Hydrogels for the Cleaning of Classic Art: A Rheological and SAXS Study. *ACS Appl. Mater. Interfaces* **2018**, *10*, 19162−19172.
(49) Scopel, E.; Rezende, C. A. Biorefinery On-Demand: Modulating Pretreatments to Recover Lignin, Hemicellulose, and Extractives as Co-Products during Ethanol Production. *Ind. Crops Prod.* **2021**, *163*, 113336.
(50) Fontoura, C. F.; Brandão, L. E.; Gomes, L. L. Elephant Grass Biorefineries: Towards a Cleaner Brazilian Energy Matrix? *J. Cleaner Prod.* **2015**, *96*, 85−93.
(51) Muñoz Viñas, S. *Teoría Contemporánea de La Restauración*; Editorial Síntesis: Madrid, 2004.
(52) Endo, K.; Obataya, E.; Zeniya, N.; Matsuo, M. Effects of Heating Humidity on the Physical Properties of Hydrothermally Treated Spruce Wood. *Wood Sci. Technol.* **2016**, *50*, 1161−1179.
(53) Weston, R. J.; Smith, G. J.; Scheele, S. M.; Williams, S. H. Accelerated Hydrothermal Degradation of Fibres of Phormium Tenax (New Zealand Flax). *J. Cult. Heritage* **2012**, *13*, 413−418.
(54) Trache, D.; Tarchoun, A. F.; Derradji, M.; Hamidon, T. S.; Masruchin, N.; Brosse, N.; Hussin, M. H. Nanocellulose: From Fundamentals to Advanced Applications. *Front. Chem.* **2020**, *8*, 392.
(55) Vardanyan, V.; Galstian, T.; Riedl, B. Effect of Addition of Cellulose Nanocrystals to Wood Coatings on Color Changes and Surface Roughness Due to Accelerated Weathering. *J. Coat. Technol. Res.* **2015**, *12*, 247−258.
(56) Tan, S.; Liu, D.; Qian, Y.; Wang, J.; Huang, J.; Yi, C.; Qiu, X.; Qin, Y. Towards Better UV-Blocking and Antioxidant Performance of Varnish via Additives Based on Lignin and Its Colloids. *Holzforschung* **2019**, *73*, 485−491.
(57) Smyth, M. *Colloidal Lignin Particles for Weathering Protection in Wood Coatings*; Aalto University: 2017.
(58) Zervos, S. Natural and Accelerated Ageing of Cellulose and Paper: A Literature Review. In *Cellulose: Structure and Properties, Derivatives and Industrial Uses*; Nova Science Publishers: 2010; pp. 1−42.
(59) Kotlík, P.; Doubravová, K.; Horálek, J.; Kubáč, L.; Akrman, J. Acrylic Copolymer Coatings for Protection against UV Rays. *J. Cult. Heritage* **2014**, *15*, 44−48.
(60) Sadeghifar, H.; Ragauskas, A. Lignin as a UV Light Blocker-a Review. *Polymers* **2020**, *12*, 1−10.
(61) Hambardzumyan, A.; Foulon, L.; Chabbert, B.; Aguié-Béghin, V. Natural Organic UV-Absorbent Coatings Based on Cellulose and Lignin: Designed Effects on Spectroscopic Properties. *Biomacromolecules* **2012**, *13*, 4081−4088.
(62) Ravichandran, R.; Cliff, N.; Renz, W. L. Light and Heat Stabilizers for Coatings. In *Handbook Of Coating Additives*; Florio, J. J., Miller, D. J., Eds.; CRC Press: 2004; p 500, DOI: 10.1201/9781482276671-12.
(63) Bojanoski, S.; Almada, M. *Illustrated Glossary of Paper Conservation: Damages and Treatments*; Fino Traço: Belo Horizonte, 2021.
(64) Debeaufort, F.; Voilley, A. Methylcellulose-Based Edible Films and Coatings: 2. Mechanical and Thermal Properties as a Function of Plasticizer Content. *J. Agric. Food Chem.* **1997**, *45*, 685−689.
(65) Senichev, V. Y.; Tereshatov, V. V. Theories of Compatibility. In *Handbook of Plasticizers:* Third *Edition*; Elsevier Inc.: 2017; pp. 135−164, DOI: 10.1016/B978-1-895198-97-3.50008-1.
(66) Panchal, P.; Ogunsona, E.; Mekonnen, T. Trends in Advanced Functional Material Applications of Nanocellulose. *Processes* **2019**, *7*, 10.
(67) Wu, L.; Liu, S.; Wang, Q.; Wang, Y.; Ji, X.; Yang, G.; Chen, J.; Li, C.; Fatehi, P. High Strength and Multifunctional Polyurethane Film Incorporated with Lignin Nanoparticles. *Ind. Crops Prod.* **2022**, *177*, 114526.
(68) Ni, S.; Bian, H.; Zhang, Y.; Fu, Y.; Liu, W.; Qin, M.; Xiao, H. Starch-Based Composite Films with Enhanced Hydrophobicity, Thermal Stability, and UV-Shielding Efficacy Induced by Lignin Nanoparticles. *Biomacromolecules* **2022**, *23*, 829−838.
(69) Lizundia, E.; Armentano, I.; Luzi, F.; Bertoglio, F.; Restivo, E.; Visai, L.; Torre, L.; Puglia, D. Synergic Effect of Nanolignin and Metal Oxide Nanoparticles into Poly(l-Lactide) Bionanocomposites: Ma-

terial Properties, Antioxidant Activity, and Antibacterial Performance. *ACS Appl. Bio Mater.* **2020**, *3*, 5263−5274.
(70) Farooq, M.; Zou, T.; Valle-Delgado, J. J.; Sipponen, M. H.; Morits, M.; Österberg, M. Well-Defined Lignin Model Films from Colloidal Lignin Particles. *Langmuir* **2020**, *36*, 15592−15602.
(71) Rao, X.; Liu, Y.; Zhang, Q.; Chen, W.; Liu, Y.; Yu, H. Assembly of Organosolv Lignin Residues into Submicron Spheres: The Effects of Granulating in Ethanol/Water Mixtures and Homogenization. *ACS Omega* **2017**, *2*, 2858−2865.
(72) Baglioni, P.; Chelazzi, D.; Giorgi, R.; Poggi, G. Colloid and Materials Science for the Conservation of Cultural Heritage: Cleaning, Consolidation, and Deacidification. *Langmuir* **2013**, *29*, 5110−5122.
(73) Dufresne, A. *Nanocellulose: From Nature to High Performance Tailored Materials*; Walter de Gruyter GmbH & Co KG: 2012, DOI: 10.1515/hf-2013-0027.
(74) Allegretti, O.; Raffaelli, F. External Resistance to Water Vapour Transfer of Varnishes on Wood. *Proceedings of the wood science and for conservation of culture heritage, Florescence*; Uzielli, L., Ed.; 2007, 92−99.
(75) Santos, S. M.; Carbajo, J. M.; Quintana, E.; Ibarra, D.; Gomez, N.; Ladero, M.; Eugenio, M. E.; Villar, J. C. Characterization of Purified Bacterial Cellulose Focused on Its Use on Paper Restoration. *Carbohydr. Polym.* **2015**, *116*, 173−181.
(76) Korhonen, O.; Forsman, N.; Österberg, M.; Budtova, T. Eco-Friendly Surface Hydrophobization of All-Cellulose Composites Using Layer-by-Layer Deposition. *eXPRESS Polym. Lett.* **2020**, *14*, 896−907.
(77) Forsman, N.; Johansson, L. S.; Koivula, H.; Tuure, M.; Kääriäinen, P.; Österberg, M. Open Coating with Natural Wax Particles Enables Scalable, Non-Toxic Hydrophobation of Cellulose-Based Textiles. *Carbohydr. Polym.* **2020**, *227*, 115363.
(78) Jeong, M. J.; Bogolitsyna, A.; Jo, B. M.; Kang, K. Y.; Rosenau, T.; Potthast, A. Deterioration of Ancient Korean Paper (Hanji), Treated with Beeswax: A Mechanistic Study. *Carbohydr. Polym.* **2014**, *101*, 1249−1254.
(79) Appelbaum, B. *Conservation Treatment Methodology*; Taylor & Francis: 2012.
(80) Xu, F.; Yu, J.; Tesso, T.; Dowell, F.; Wang, D. Qualitative and Quantitative Analysis of Lignocellulosic Biomass Using Infrared Techniques : A Mini Review. *Appl. Energy* **2013**, *104*, 801−809.
(81) Hergert, H. L. Infrared Spectra of Lignin and Related Compounds. II. Conifer Lignin and Model Compounds1,2. *J. Org. Chem.* **1960**, 405.
(82) Rashid, T.; Kait, C. F.; Murugesan, T. A "Fourier Transformed Infrared" Compound Study of Lignin Recovered from a Formic Acid Process. *Procedia Eng.* **2016**, 1312.
(83) Appelbaum, B. Criteria for Treatment: Reversibility. *J. Am. Inst. Conserv.* **1987**, *26*, 65−73.

https://doi.org/10.1021/acsanm.2c02968
ACS Appl. Nano Mater. 2022, 5, 13245−13259